Pattern formation in binary fluid mixtures induced by short-range competing interactions

Cecilia Bores,[1] Enrique Lomba,[1,2,a)] Aurélien Perera,[2] and Noé G. Almarza[1]
[1]*Instituto de Química Física Rocasolano, CSIC, Serrano 119, E-28006 Madrid, Spain*
[2]*Laboratoire de Physique Théorique de la Matiére Condensée (UMR CNRS 7600), Université Pierre et Marie Curie, 4 Place Jussieu, F75252 Paris Cedex 05, France*

(Received 29 June 2015; accepted 23 July 2015; published online 24 August 2015)

Molecular dynamics simulations and integral equation calculations of a simple equimolar mixture of diatomic molecules and monomers interacting via attractive and repulsive short-range potentials show the existence of pattern formation (microheterogeneity), mostly due to depletion forces away from the demixing region. Effective site-site potentials extracted from the pair correlation functions using an inverse Monte Carlo approach and an integral equation inversion procedure exhibit the features characteristic of a short-range attractive and a long-range repulsive potential. When charges are incorporated into the model, this becomes a coarse grained representation of a room temperature ionic liquid, and as expected, intermediate range order becomes more pronounced and stable. © *2015 AIP Publishing LLC.* [http://dx.doi.org/10.1063/1.4928524]

I. INTRODUCTION

Spontaneous pattern formation is a feature present in a diverse collection of physical, chemical, and biological systems.[1] In spite of the diverse nature of these systems, the appearance of the emerging microphases is quite similar: in 2D systems, circular droplets, stripes, or "bubbles" occur, and in 3D systems, one may find spherical droplets, sheets, or tubes. In some cases, the patterns appear as transient states due to energy or mass fluctuations that occur in the process of spinodal decomposition, but sometimes, these states can be stabilized due to the presence of competitive interactions, in which one of the interactions is responsible for inhibiting the phase separation.[2,3]

The understanding of this self-organizing capability of soft and fluid matter is critical for a wide panoply of applications of great relevance nowadays. These self-assembly mechanisms play a crucial role in processes involving protein solutions in food products,[4,5] therapeutic monoclonal antibodies,[6–8] nanolithography,[9] or gelation processes.[10]

In the realm of colloidal science, systems with extremely short ranged repulsive interactions are often used as an experimental realization of the hard sphere fluid,[11] a system notorious for its theoretical interest. On the other hand, the addition of non-adsorbing polymers to the colloidal solution typically activates an attractive inter-particle interaction, due to the depletion mechanism. Moreover, changing the concentration and molecular weight of the polymer, the attraction range and strength of the colloid-colloid interaction can be tuned. Clustering is to be expected due to the presence of the attractive forces,[12,13] but in principle, it would correspond to meta-stable states and/or irreversible processes of kinetic nature. Nevertheless, microphases formed by clusters and percolating structures can be stabilized in protein solutions and colloid-polymer mixtures both in experiment[14] and in theoretical descriptions[15] due to the presence of additional repulsive interactions stemming from electrostatic forces. An extreme example of the stabilizing role of charges is the nanostructural organization that appears in room temperature ionic liquids (RTILs).[16] In fact, it has been shown that long range repulsive interactions alone can give rise to nanostructural order,[17] the driving force of attractive interactions to induce spontaneous aggregation being replaced by external forces (e.g., pressure).

In the case of colloidal systems, in which charged colloidal particles are screened by ions in the solvent, the colloid-colloid interaction has been shown on theoretical grounds to be adequately represented by a Yukawa potential[18,19] according to the Derjaguin-Landau-Verwey-Overbeek (DLVO) theory. Following this, numerous works have resorted to potentials with a combination of a short range attraction and a long range repulsion (SALR) in the form of a double Yukawa,[20,21] or a Lennard-Jones (LJ) plus a Yukawa interaction[2,22,23] in order to model the spontaneous emergence of microstructured patterns in fluids. On the other hand, back in 1999, Sear *et al.*[24] made use of an empirical two exponential form with SALR characteristics in order to explain the experimental appearance of stable microphases of nanoparticles at the air-water interface. This potential has been studied in depth in model systems, both in bulk and in confinement,[25–29] and as a rough approximation to account for vegetation patterns in ecosystems with limited resources.[30]

In this work, we will explore the possibility of pattern formation in a system in which only short ranged forces are present. Our model system, composed of heteronuclear dimers and monomers, combines attractive and repulsive potentials so as to mimic the interactions present in RTILs, but without electrostatic forces. To that aim, we have performed extensive molecular dynamics simulations in the canonical and in the isothermal-isobaric ensembles. We will address the emergence of intermediate range order (IRO) analyzing the behavior of the

a)enrique.lomba@csic.es

partial and concentration-concentration structure factors and performing a cluster analysis for various degrees of asymmetry in the sites of the diatomic particles. Reference Interaction Site Model (RISM) integral equation calculations have also been carried out and are shown to agree remarkably well with the simulation results. By means of an Inverse Monte Carlo (IMC) approach,[31] we have extracted effective interactions from the pair correlation functions of the simulated mixtures. For comparison, another set of effective potentials has been obtained from the RISM results using an integral equation inversion procedure. We will see that despite the fact that all interactions at play are short ranged, their net effect leading to the pattern formation (microheterogeneity, or microstructure segregation at the nanoscale) translates into the appearance of effective interactions that agree with the characteristic trends of a short range attraction and a long range repulsion, i.e., a SALR potential. We have found that the effective potentials extracted from the simulation and those derived by the theoretical approach agree remarkably well. Finally, we have analyzed the role of charges on our model, which in fact by the addition of electrostatic site-site interactions becomes a rough representation of a RTIL. As expected, charges will be shown to enhance the pattern formation and the stability of the nanostructured phases.

The rest of the paper can be sketched as follows. In Sec. II we introduce the model in full detail and briefly summarize the methodology. In Section III, we introduce our most significant results. Conclusions and future prospects are to be found in Section IV.

II. MODEL AND METHODS

Our model consists in an equimolar fluid mixture of two different species, a two-site dimer AB and a monomer C. The dimers are represented by a two center LJ site-site potential, in which the sites are separated by a distance l. Our monomers also interact via LJ potentials. In all cases, the interactions are cut and shifted at a distance r_c, by which the explicit form of the site-site potentials is

$$u_{ij}(r) = 4\epsilon \left[\left(\frac{\sigma_{ij}}{r}\right)^{12} - \left(\frac{\sigma_{ij}}{r}\right)^{6} - \left(\frac{\sigma_{ij}}{r_c}\right)^{12} + \left(\frac{\sigma_{ij}}{r_c}\right)^{6} \right] \quad \text{if } r < r_c, \tag{1}$$

and $u_{ij}(r) = 0$ otherwise. Our model is to a certain degree inspired by the simple coarse-grained model for imidazolium based RTIL of Merlet *et al.*[32] We will see to what extent a simple model, with just two sites and purely short ranged interactions can reproduce the presence of nano-structural order as found in RTILs. To that aim, we will however preserve the attractive/repulsive character of the interactions in the RTIL. In our model then, C monomers would correspond to anions, AB dimers to the molecular cations, with the imidazolium ring that contains the positive charge, being represented by site A, and the non-polar tail, by the larger site B. This implies that AA and CC interactions will be repulsive, BB and AC are attractive, finally BC and AB interactions are also repulsive. For the sizes of A and C particles, we have chosen $\sigma_{AA} = \sigma_{CC} = 4$ Å, the elongation of the dimer $l = 8$ Å. The AB distances of the dimers are fixed as constraints of the equations of motion. The LJ well is set to $\epsilon = 2.092$ kJ/mol, identical for all interactions. Since the size of the non-polar tail is essential to determine the nanostructural ordering,[16] we have considered various sizes for σ_{BB} (with $\sigma_{BB} > \sigma_{AA}$ always). For the attractive interactions, we have truncated and shifted the LJ potential at $r_c = 3\sigma_{BB}$. For the repulsive interactions, we have simply used $r_c = 2^{1/6}\sigma_{ij}$, thus defining purely repulsive soft spheres following the prescription of Weeks, Chandler, and Andersen (WCA).[33] The complete set of parameters for all interactions is summarized in Table I. Finally, in order to analyze the effect of charges on the intermediate range order, we have considered explicitly the same model with a positive charge $+q$ on the A sites and a corresponding negative charge $-q$ on the monomers. The value of q is varied between 0 and $0.25e$, where e is the elementary electron charge. Again these values are of the same order as those considered in the model of Ref. 32.

TABLE I. Lennard-Jones potential parameters.

Particle i	Particle j	Interaction	ϵ (kJ/mol)	σ_{ij}	r_c
A	A	Repulsive	2.092	4.0 Å	$2^{1/6}\cdot\sigma_{AA}$
A	B	Repulsive	2.092	$(\sigma_{AA}+\sigma_{BB})/2$	$2^{1/6}\cdot\sigma_{AB}$
A	C	Attractive	2.092	4.0 Å	$3\cdot\sigma_{BB}$
B	B	Attractive	2.092	σ_{BB}	$3\cdot\sigma_{BB}$
B	C	Repulsive	2.092	$(\sigma_{BB}+\sigma_{CC})/2$	$2^{1/6}\cdot\sigma_{BC}$
C	C	Repulsive	2.092	4.0 Å	$2^{1/6}\cdot\sigma_{CC}$

A. Simulations and analysis

We have carried out extensive molecular dynamics simulations of the system previously described using the LAMMPS package,[34–36] in the canonical and isothermal-isobaric ensembles using a Nose-Hoover thermostat and barostat.[37] Our samples contained 16 384 particles (samples of up to 65 536 particles were investigated and no significant size dependence was found). For simplicity, we considered equal masses for the three interaction centers: $m_A = m_B = m_c = 16$ g mol^{-1}. Initial thermalization runs at a temperature of 226 K were 2×10^6 steps long, with a time step of 1 fs. Production runs were 5×10^6 steps long, and averages were carried out every 5000 steps.

One of the problems one can encounter when performing canonical simulations in this type of system is the occurrence of phase transitions, either vapor-liquid equilibria or demixing. In order to guarantee that the states under consideration correspond to thermodynamic equilibrium conditions, and consequently, any potential intermediate range order is not the result of a spinodal decomposition, we have run additional isothermal-isobaric simulations and analyzed the volume fluctuation of the samples. In this way, one can avoid those states that lie inside the liquid-vapor spinodal. Moreover, one can compute the partial structure factors, defined as

$$S_{ij}(\mathbf{k}) = x_i\delta_{ij} + x_i x_j \rho \int \left(g_{ij}(r) - 1\right) e^{-\mathbf{kr}} d\mathbf{r}, \tag{2}$$

where ρ is the total number density, δ_{ij} is a Kronecker δ, and x_i is the molar fraction of component i. Here, sites A and B are considered as different particles and g_{ij} is the atom-atom

pair distribution function. Our samples are large enough to allow for an accurate integration of the pair distribution functions, and the results are consistent with direct k-sampling. Notice that as far as Eq. (2) is concerned, $x_A = x_B = x_C = 1/3$; hence, in the large k limit, all structure factors will tend to 1/3. From the partial structure factors, it is possible to evaluate the concentration-concentration structure factor introduced by Bathia and Thornton,[38] for which we have defined

$$S_{cc}(k) = x_{AB}^2 S_{CC}(k) + x_C^2 S_{AB-AB}(k) - 2x_{AB}x_C S_{C-AB}(k), \tag{3}$$

where now one has to consider explicitly the structure factors corresponding to the molecular species AB, and as a consequence, $x_C = x_{AB} = 1/2$. We can simply approximate $g_{AB-AB} = g_{BB}$ and $g_{C-AB} = g_{CB}$, as if the scattering length or form factor of A sites was negligible compared to that of B sites. This is in principle not unreasonable given the much larger size of the B sites, but in a realistic situation, one should take explicitly into account the true scattering lengths or form factors of sites A and B. Now, one has to correct for the different values of the molar fraction when AB is considered as a single species and Eq. (2) is used in (3). In this way, $\lim_{k\to\infty} S_{cc}(k) = x_c x_{AB} = 1/4$. With all this in mind, the presence of a divergence when $k \to 0$ in $S_{cc}(k)$ is a signal of a demixing transition, so this quantity will be essential to assess the stability of the thermodynamic states chosen for our simulations.

Finally, back to the vapor-liquid transition, one can analyze the corresponding k-dependent linear response susceptibility in density fluctuations, namely,[39]

$$\rho k_B T \chi_T(k) = \frac{|\mathbf{S}(k)|}{\sum_{ab}(x_a x_b)|\mathbf{S}(k)|_{ab}}, \tag{4}$$

whose $k = 0$ limit is precisely the isothermal compressibility. In Eq. (4), k_B is Boltzmann's constant, T the absolute temperature, and the elements of the matrix $\mathbf{S}_{ij}$ are just the partial structure factors as defined in Eq. (2). $|\ldots|$ denotes the matrix determinant and $|\ldots|_{ab}$ the corresponding minor of the matrix $\mathbf{S}(k)$. The presence of a divergence—or a substantial increase in $\chi_T(0)$—is a clear indication of the vicinity of a vapor-liquid transition. A careful monitoring of this quantity together with the use of NPT simulations provides a reliable assessment of the stability of the state points under consideration during the simulation runs.

All systems and conditions studied in this work are summarized in Table II. In the case of system 8, when increasing the charge from $0.10e$ to $0.25e$, the conditions of temperature and density corresponding to systems 3, 6, and 7 lie in the two-phase region. Consequently, we resorted to an isothermal-isobaric simulation at low positive pressure to achieve thermodynamic equilibrium conditions in our system with $q = 0.25e$. The final value of the total particle density achieved in this way is indicated in Table II.

TABLE II. Potential parameters and thermodynamic state variables for the systems under study.

	Potential thermodynamic state				
	$\|q\|(e)$	σ_B (Å)	ρ (Å^{-3})	T (K)	P (MPa)
System 1	0	8.0	0.001	226.4	27.05
System 2	0	8.0	0.001 25	226.5	39.5
System 3	0	8.0	0.001 5	226.5	59.4
System 4	0	9.0	0.001	226.5	30.4
System 5	0	9.0	0.001 25	226.4	53.2
System 6	0	9.0	0.001 5	226.4	96.7
System 7	0.1	8.0	0.001 5	226.4	39.4
System 8	0.25	8.0	0.001 95	226.3	0.61

B. Inverse Monte Carlo method

With the pair correlation functions produced along the simulation runs and the corresponding statistical uncertainties calculated using block averages, we have used the IMC procedure proposed by Almarza and Lomba[31] in order to produce single component site-site effective potentials able to reproduce the microscopic structure exhibited by our mixture model. The procedure starts from a simple approximation $\beta u_{in}^{eff}(r) = -\log g(r)$ and proceeds to modify the pair potential along the simulation run in such a way that the calculated $g^{eff}(r)$ matches the input $g(r)$. Explicit details of the method can be found in Ref. 31. In our case, we have used a total of 4000 particles. The procedure of inversion was carried out in 20 stages. In the last stages, the effective potentials hardly varied, and the convergence between input and calculated $g(r)$'s according to the prescription of Ref. 31 was achieved successfully in all the cases.

In this way, one can use as input of the IMC procedure either $g_{AA}(r)$, $g_{BB}(r)$, or $g_{CC}(r)$ and obtain a corresponding set of $u_{AA}^{eff}(r)$, $u_{BB}^{eff}(r)$, and $u_{CC}^{eff}(r)$, which will obviously be different, but in the case of emergence of intermediate range, order should exhibit some common features.

C. RISM integral equation

The site-site correlations are obtained by solving the usual set of 2 equations, the site-site Ornstein-Zernike (SSOZ) equation and the closure equation, which we choose here to be the site-site hypernetted (SS-HNC) equation. The SSOZ equation for the present system is explicitly given in the matrix form

$$(\mathbf{W} + \frac{\rho}{3}\mathbf{H})(\mathbf{W}^{-1} - \frac{\rho}{3}\mathbf{C}) = \mathbf{I}, \tag{5}$$

where the 3×3 matrix $\mathbf{H}$ (or $\mathbf{C}$) has for elements $H_{ij} = \tilde{h}_{ij}(k)$ (or $\mathbf{C}_{ij} = \tilde{c}_{ij}(k)$), the Fourier transform (FT) of the site-site pair correlation functions $h_{ij}(r) = g_{ij}(r) - 1$ (or the direct correlation function $c_{ij}(r)$), where the indices i and j stand for one of the sites A, B, and C. The matrix $\mathbf{W}$ represents the intramolecular correlations, which for the present system gives

$$\mathbf{W} = \begin{pmatrix} \tilde{w}_{AA} & \tilde{w}_{AB} & \tilde{w}_{AC} \\ \tilde{w}_{AB} & \tilde{w}_{BB} & \tilde{w}_{BC} \\ \tilde{w}_{AC} & \tilde{w}_{BC} & \tilde{w}_{CC} \end{pmatrix} = \begin{pmatrix} 1 & j_0(kl) & 0 \\ j_0(kl) & 1 & 0 \\ 0 & 0 & 1 \end{pmatrix}, \tag{6}$$

where $j_0(x)$ is a spherical Bessel function. The matrix $\mathbf{I}$ is the identity matrix. The SS-HNC equations are written as

$$g_{ij}(r) = \exp\left[-\frac{u_{ij}(r)}{k_B T} + h_{ij}(r) - c_{ij}(r)\right], \tag{7}$$

and there are 9 such independent equations to solve.

Both equations are approximate and their respective inconsistencies have been discussed many times in the past literature.[39,40] Based on empirical evidence from the literature, we expect that the correlations obtained through these equations for the present systems, both charged and uncharged, should be relatively good for the short range part, but perhaps not at long range. We are particularly interested to see if the correlations related to the appearance of the local structures can be reproduced by this theory. The structure factor defined in Eq. (3) is the appropriate function for this purpose, as illustrated in Sec. III.

The practical solution of these equations consists in discretizing all the functions on an equidistant grid, both in r and k space. We use 2048 points with a r-grid of $\Delta r = 0.01\sigma_A$, which is enough for the present case to properly describe the asymptotic behavior of the correlations in direct and reciprocal space. The set of two equations are solved iteratively following techniques well documented in the literature.

It is also possible to obtain the effective potentials which would correspond to the equivalent one-component representation of the system. This is achieved by imposing the pair correlation function to be the desired site-site correlation, namely, $g(r) = g_{XX}(r)$, in the set of the two integral equations for the 1-component system and solve these equations for the direct correlation function and effective pair interaction. The direct correlation function can be obtained through the OZ equation for 1-component system (which is an exact relation),

$$(1 + \rho_S \tilde{h}(k))(1 - \rho_S \tilde{c}(k)) = 1, \tag{8}$$

where $h(r) = g(r) - 1 = h_{XX}(r) = g_{XX}(r) - 1$, and the density ρ_S is that of the effective 1 component made solely of sites X. Once $c(r)$ is obtained, one solves the HNC closure, which has the same form as Eq. (7), but now for the effective interaction $u_{eff}(r)$, one gets

$$u_{eff}(r) = -k_B T \left[\ln g_{XX}(r) + h_{XX}(r) - c(r)\right]. \tag{9}$$

III. RESULTS

A. Pair structure

Here, we have analyzed the effect of the molecular geometry on the nanostructure formation changing the diameter of σ_{BB}. We have first considered $\sigma_{BB} = 8$ Å, 9 Å, 10 Å, and 12 Å. Some snapshots of configurations for varying σ_{BB} are depicted in Figure 1. We have found that for $\sigma_{BB} > 9$ Å, clustering or microheterogeneity of C particles can only be appreciated when the packing of the B sites is so high that it resembles that of a solid. In fact in this case, the height of the first peak of $S_{BB}(k)$ exceeds 2.7, which according to the Hansen-Verlet rule[41] indicates that freezing conditions have been reached. Moreover, the prepeak in the structure factor characteristic of the presence of IRO is absent from $S_{BB}(k)$. The clustering of C particles results from a merely steric effect, since these are restricted to occupy the holes between the large B particles. These effects can be appreciated in the snapshots of Figure 1, where the dense packing of B sites (red spheres) is readily apparent.

For the reason mentioned above, we will concentrate on the results for $\sigma_{BB} = 8$ Å and 9 Å. Already in the corresponding snapshot of Figure 1, one can appreciate the formation of a bicontinuous network of percolating clusters, connecting both AB dimers and C monomers. By bicontinuous network, we mean that the clusters formed by B-sites and C particles will be seen to both span practically the whole sample, forming two continuous interpenetrated percolating microphases. This can be analyzed from a more quantitative perspective by first taking a look at the corresponding pair distribution functions and partial structure factors, which are depicted in Figures 2 and 3, respectively, for Systems 1–6. Focusing first on the g_{AA} pair distribution function, one first appreciates the large exclusion hole after the first layer, which is a simple consequence of the large size of B-sites. Obviously, the exclusion hole grows with the size of the B-sites, as can be seen when comparing figures

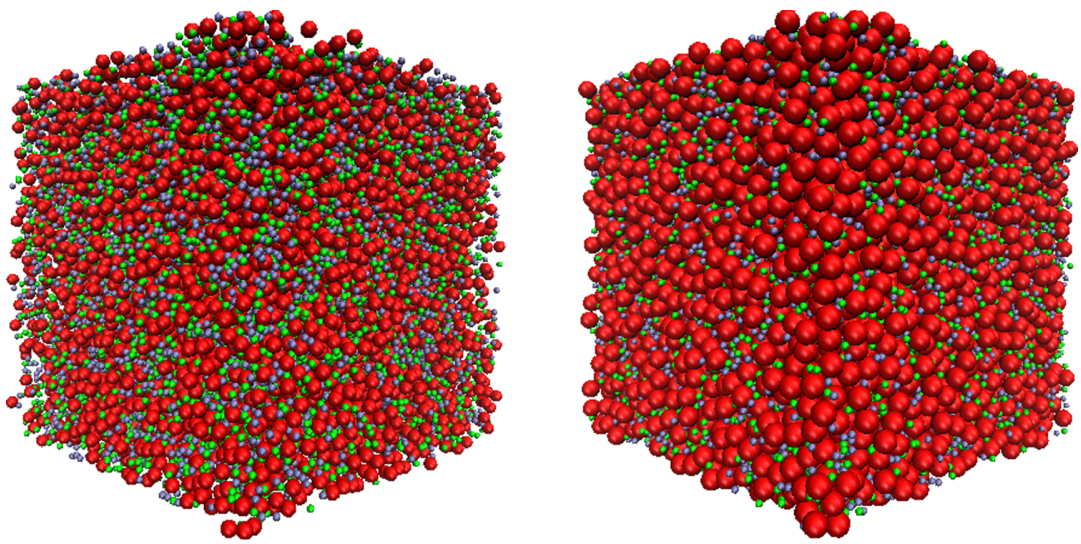

FIG. 1. Snapshots of configurations for total particle density $\rho = 0.001\,25$ Å^{-3} and temperature $T = 226.45$ K for two B-site diameters. As the size of B-sites grows, C monomers cluster in the cavities formed by the B-sites due to excluded volume effects. All other diameters and total density are kept fixed, $\sigma_{AA} = \sigma_{CC} = 4.0$ Å. (a) $\sigma_{BB} = 8$ Å. (b) $\sigma_{BB} = 12$ Å.

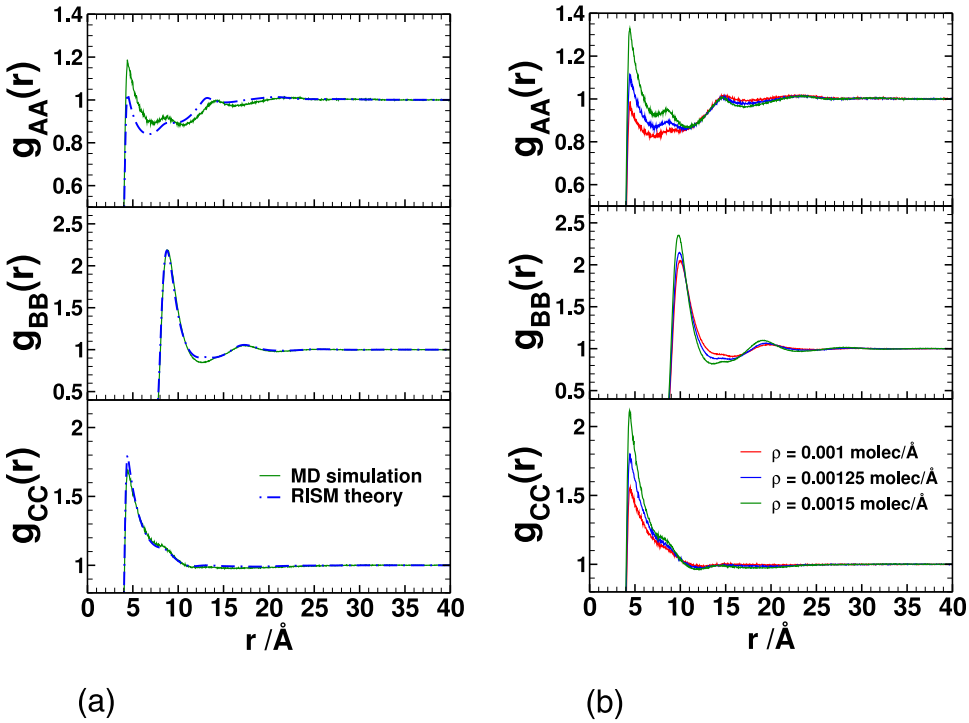

FIG. 2. The figures show the radial distribution functions for A, B, and C particles, respectively. Column (a) corresponds to $\sigma_{BB} = 8$ Å for system 3 (theory vs. simulation) and column (b) presents the simulations results for systems 4–6 for $\sigma_{BB} = 9$ Å. Total density is indicated in the legend. Simulation results are represented by solid lines and dashed-dotted curves correspond to integral equation calculations.

on the left and right columns. Correlations between A-sites extend up to five σ_{AA}, and the width of the g_{CC} correlation is $\approx 2\sigma_{CC}$. These features hint at the presence of some degree of IRO. B-B correlations (graphs in the middle row) behave like those of a dense fluid, and no apparent sign of clustering or IRO is evident. In contrast, the wide first peak of g_{CC} is characteristic of clusters of particles confined in cavities, in this case formed by B-sites. This effect, as mentioned before, is maximized for the largest σ_{BB}. We will see later that these clusters of partly occluded C-particles are connected, forming a three dimensional percolating structure.

If we take now a look at the partial structure factors, we immediately appreciate a feature characteristic of the emergence of IRO, namely, the presence of a prepeak at 0.25 Å $^{-1}$. This corresponds to correlations in the range of 25 Å, the distance at which any sign of structure of the pair distribution function dies out. Interestingly, the prepeak is almost absent in S_{AA}, except for a small maximum visible for the $\sigma_{BB} = 9$ Å and the highest density. This quantity shows otherwise very little structure for $k > 0.5$ Å^{-1}. As seen in the g_{AA}'s, the most relevant feature in the AA correlations is the exclusion hole due to the presence of the B-sites. In contrast, S_{BB} does exhibit a prepeak, even when no evidence of IRO was visible in g_{BB}. This prepeak is more apparent in the monomer structure factor S_{CC}. When the density is lowered, the prepeak in the B-site structure factor shifts to lower k-values and vanishes at $\rho = 0.001$ Å^{-3}. In the case of S_{CC}, the position of the prepeak is preserved, but its magnitude decreases. In Figure 4, the corresponding concentration-concentration structure factor is displayed. The prepeak at $k_0 \approx 0.25$ Å^{-1} is preserved, although its magnitude decreases when the total density is lowered. In contrast, no increase when $k \to 0$ is visible. This implies that we are encountering concentration fluctuations inducing spatial inhomogeneities, but no demixing transition. In Figure 5, we have plotted the k-dependent susceptibility corresponding to density fluctuations. The prepeak is visible except for the lowest density, which implies that density inhomogeneities with a spatial patterns are also correlated with the corresponding concentration inhomogeneities. But now, the $k \to 0$ behavior is different. As density is decreased, the susceptibility (i.e., the isothermal compressibility) grows, an indication of the vicinity of a vapor-liquid transition. This means, that lowering the density from the value of $\rho = 0.001$ Å^{-1} at the same temperature could move the system across the spinodal curve into the two-phase region. Our analysis indicates that the thermodynamic conditions we have simulated can be considered equilibrium states. Moreover, we have confirmed that the results do not have a significant sample size dependence, by which metastability can also be ruled out.

The site-site correlation functions and structure factors obtained from the RISM theory are represented in dashed lines in Figs. 2-3. It is seen that the agreement is excellent in most cases, particularly in what concerns the BB and CC correlations. The AA correlations are systematically underestimated near contact and overestimated at larger distances. The most significant differences are seen for the structure factors in Fig. 3. Integral equations tend to exaggerate concentration fluctuations and often tend to interpret small aggregate formations as such.[42,43] We observe here a similar trend for the low density case $\rho = 0.001$ Å^{-3}, for which fluctuations compete the most with aggregate formation. The prediction of aggregation, through the prepeak is in very good agreement with simulations for the highest density $\rho = 0.0015$ Å^{-3}, precisely when the denser packing tends to favor aggregation. This is also in line with previous observations of similar type of behavior for model ionic liquids. These features are a direct consequence of the fact that the HNC closure approximation misses high order correlations, hence high order cluster contributions, which are represented in the bridge term $b_{ij}(r)$ that is neglected in the exponential of Eq. (7). We observe that in all cases, the k = 0

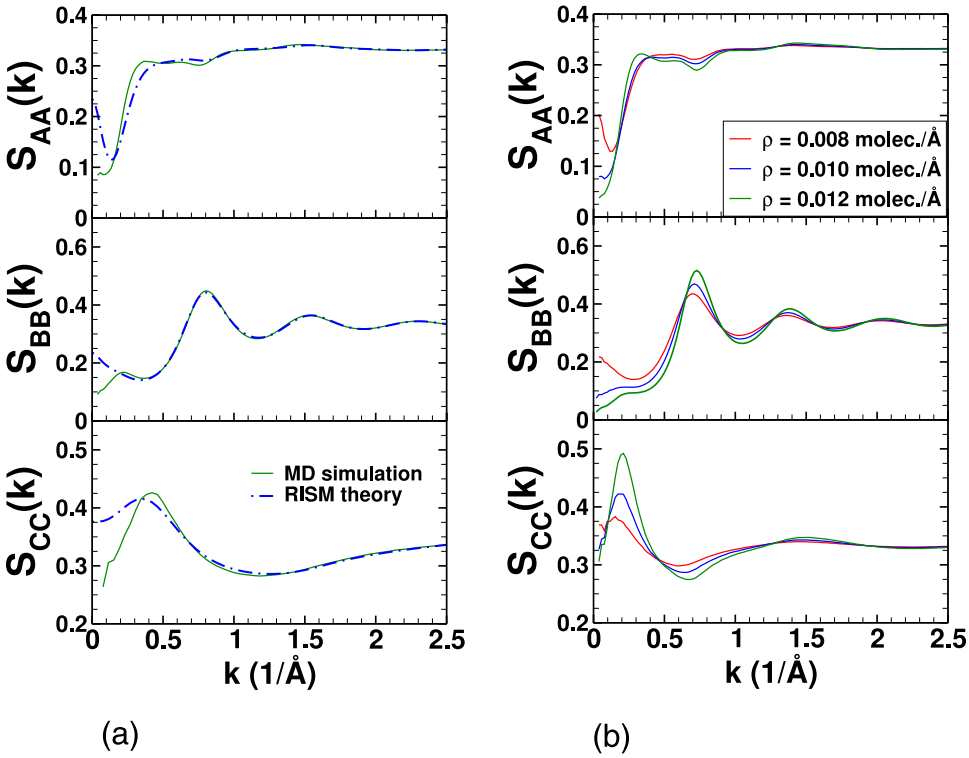

FIG. 3. The figures show the structure factors for A, B, and C particles, respectively. Column (a) corresponds to $\sigma_{BB} = 8$ Å for system 3 (theory vs. simulation) and column (b) presents the simulations results for systems 4–6 for $\sigma_{BB} = 9$ Å. Total density is indicated in the legend. Simulation results are represented by solid lines and dashed-dotted curves correspond to integral equation calculations.

behavior of the RISM structure factor always overestimates the concentration fluctuations.

B. Effective pair potentials

In Figure 6, we present the effective potentials obtained from the site-site pair distribution functions. By construction, using these effective potentials in a simulation for a single component system will lead to a pair distribution function coincident with the original site-site correlation of the mixture. This is one of the possible alternatives to reduce the behavior of a complex system to a simpler one component system. Other alternatives, such as the force-matching approach,[44] will lead to quantitatively different results, but certainly retaining the essential features of the effective potentials found here. Among these features, we see that in all cases, the effective potential has a short range (extremely short in the case of AA potentials) attractive well and this is followed by a long range repulsive region, which extends to 20-30 Å. The repulsive region of U_{CC}^{eff} is much less visible and is illustrated in the inset. The repulsive range is more influenced by the change in the total density. The attractive part of AA and CC effective interactions is due to depletion forces (in this case, the plain site-site interactions are repulsive). In the case of AA interactions, most of the attractive wells are masked by the excluded volume effect of the B sites in the AB molecules (the large repulsive potential between 5-15 Å corresponds to the exclusion hole in g_{AA}). Note that even if in g_{BB} long range correlations due to nanostructure organization are clearly not visible, there are long range repulsions in the BB effective potential, which are reflected in the prepeak in S_{BB} as an indication of IRO. The long range repulsion vanishes for $\rho = 0.001$ Å^{-3}, which we have seen is a state approaching the gas-liquid transition.

Fig. 6 shows the effective pair potentials as obtained by the integral equation approach outlined in Section II C. The comparison with the simulations is overall quite good in all

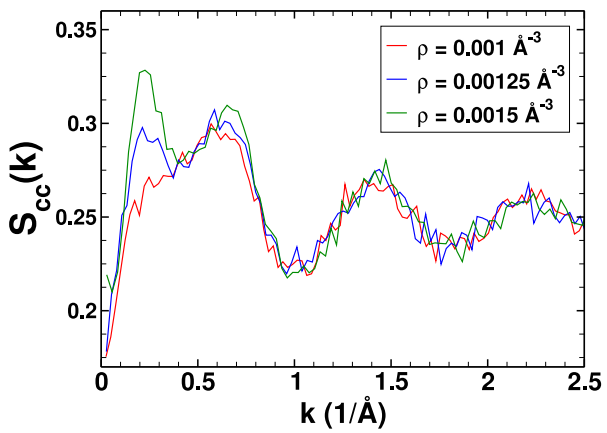

FIG. 4. Concentration-concentration structure factor for the systems 1–3.

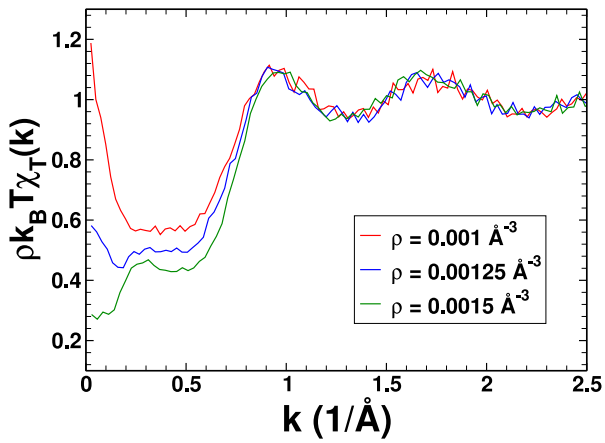

FIG. 5. Isothermal compressibility as a function of k for systems 1–3.

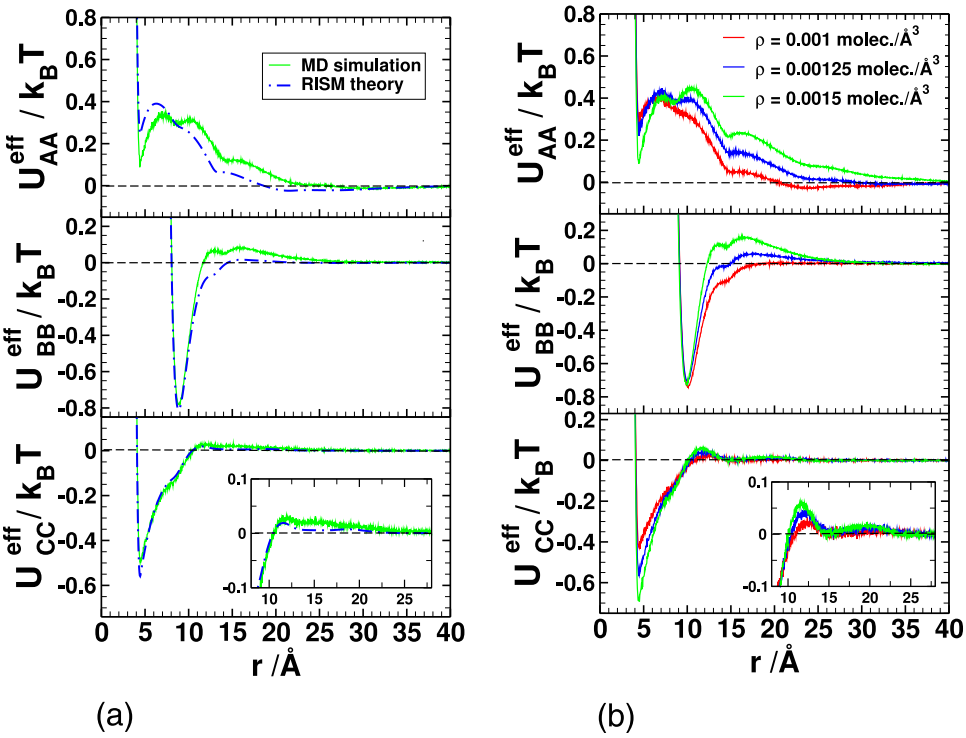

FIG. 6. Effective potentials for A, B, and C particles, respectively. Column (a) corresponds to $\sigma_{BB} = 8$ Å for system 3 (theory vs. simulation) and column (b) presents the simulations results for systems 4–6 for $\sigma_{BB} = 9$ Å. Total density is indicated in the legend. Simulation results are represented by solid lines and dashed-dotted curves correspond to integral equation calculations.

cases. However, it is seen that the repulsive shoulder-which is the signature of the clustering ability-is always systematically underestimated by the theory. This is a direct consequence of the weaker tendency of the integral equation theory to predict clustering.

Taken into account that B-sites are much larger than A-sites, we can think of our model as a system of B particles in a "sea" of C monomers, just like colloids in solution. Following the work of Mani *et al.*,[23] we can use a functional form of the type

$$U(r)/k_BT = 4a_0\left[\left(\frac{\sigma_{BB}}{r}\right)^{12} - \left(\frac{\sigma_{BB}}{r}\right)^{a_1}\right] + \frac{a_2 a_3}{r} e^{-\frac{r}{a_3}} \qquad (10)$$

to represent the BB effective interactions. Note that given the large size of the B-sites, we have retained the repulsive part of the bare LJ interaction in order to account for the repulsive component of the effective potential. One can see that the fits of the effective interactions $U^{eff}_{BB}/(k_BT)$ to Eq. (10) represented in Figure 7 are fairly accurate except for the minor inflection of the curve around 13 Å. The parameters of the fit are collected in Table III. Notice that the exponent of the attractive LJ component, a_1, deviates substantially from the standard value of 6, being its range shorter as density increases. The range parameter a_3 grows considerably with the density, reflecting the increase of intermediate range ordering as the total density is increased. We observe that a single component representation of our system can be well performed by a standard SALR potential in which the long range repulsion has the form of a Yukawa interaction, even when the original bare interactions in the mixture are relatively short ranged LJ potentials.

C. Cluster analysis

In order to go beyond the mere qualitative information provided by simulation snapshots and the two-body level information furnished by pair distribution functions or site-site structure factors, we have also performed a geometric cluster analysis on the B sites and the C monomers, using different values for the link distance r_{cl}. Essentially, this distance defines two particles as linked, and in this work, it has been defined in terms of the position of the inflection point

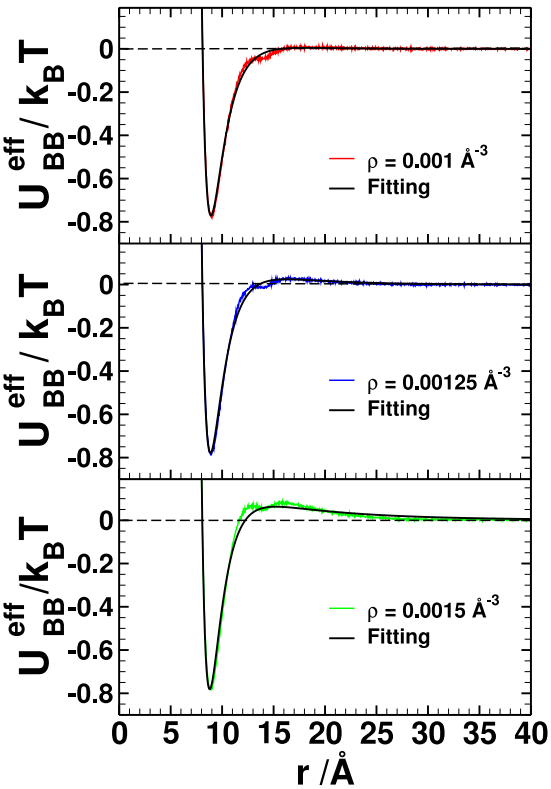

FIG. 7. B-B effective interaction for systems 1–3, fitted to a generalized LJ+Yukawa interaction.

TABLE III. Parameters of SALR effective interaction (10) between B sites fitted to the data extracted from the IMC procedure. Note that the potential is scaled with k_BT, by which a_0 is dimensionless.

	a_0	a_1	a_2 (Å)	a_3 (Å)
System 1	1.788	8.185	3.749	4.297
System 2	2.066	8.667	0.843	7.282
System 3	3.578	9.927	0.231	14.816

of the corresponding effective potentials depicted in Figure 6. We will use various values of r_{cl} in the range 10-12 Å for B-sites and C monomers and 6-8 Å for A-sites. The effects of the particular choice of r_{cl} on the cluster distribution will be analyzed. Specifically, we have calculated the normalized cluster size distribution, $N(s)$, as proposed by Stauffer.[45] This quantity is defined as the fraction of particles contained in clusters of size s, i.e., $N(s) = n(s)(s/N)$, where $n(s)$ is the number of clusters of size s. With this definition, $\sum N(s) = 1$. Of all the systems analyzed, in Figure 8, we have chosen to plot the results of system 6, which exhibits a significant prepeak in its partial structure factors. We observe that the normalized cluster size distributions of both A and B-sites and C monomers present the same qualitative features: first, one finds a maximum for isolated particles which decays monotonously to zero at a value of cluster size, s, that strongly depends on r_{cl}. This is a typical behavior of a non-associating fluid, in which instantaneous clusters are created and destroyed as particles explore their configurational space. If stable finite clusters were formed, the cluster size distribution should exhibit the

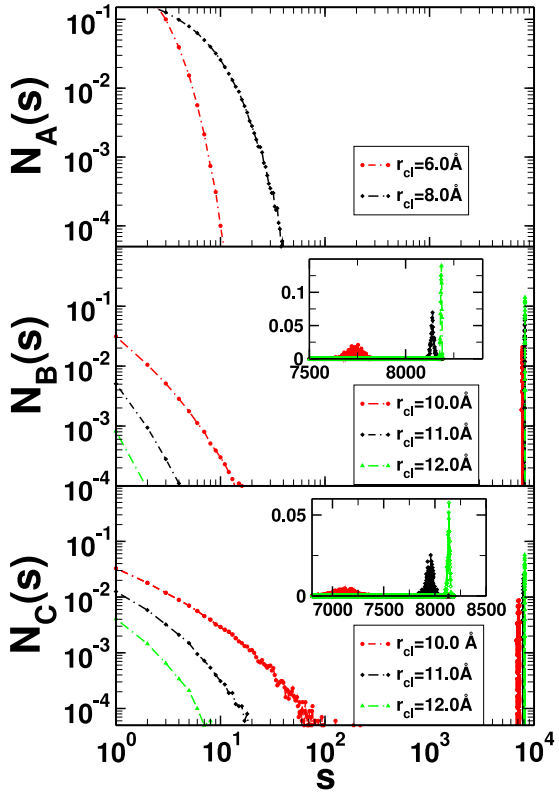

FIG. 8. Normalized cluster distribution function for A and B sites and C monomers of system 3.

corresponding maxima for the preferred sizes. On the other end of the s-axis, interestingly, one finds large clusters that span all the simulation cell. Here, $N(s)$ shows little dependence on r_{cl}, particularly for the B-sites and C monomers. Finally, the cluster size distribution of A and B sites is qualitatively very similar, which is understandable taking into account that both sites are linked into single molecular units. In Sec. III D, we will see that this symmetry is broken by the presence of charges and a new symmetry between A-sites and C particles emerges.

Thus, from our analysis, a more clear picture shows up, in which we have a large portion of the sample linked into microsegregated clusters forming bicontinuous structures, with a remnant of disconnected particles that form short lived structures up to tens or hundreds of particles depending on the choice of r_{cl}, as one would expect in a non-associating fluid.

D. The effect of charges

Our previous results have shown that microheterogeneity or stable intermediate range order can be induced by competing short range interactions in a simple mixture model of dimers and monomers. Our model was somehow inspired by a coarse grained representation of ionic liquids, which are in reality characterized by the presence of Coulombic interactions, absent from our model. An immediate question that deserves to be answered is then how the presence of charges affect the stability of the aforementioned bicontinuous structures. To that aim, we have carried out the corresponding analysis on systems 7 and 8 that, as mentioned, correspond to system 3 with charges $+q$ added to sites A and $-q$ to the C monomers. For $q = 0.1e$, standard canonical molecular dynamics simulations were run. Recall that in the case of $q = 0.25e$, density had to be increased in order to move out of the vapor-liquid coexistence region. This was simply achieved by means of an isothermal-isobaric simulation run at the same T as the original system and a pressure of 0.61 MPa, leading to a total $\rho = 0.001\,95$ Å^{-3}. In the snapshots of Figure 9, one can readily see that the charges enhance the formation of microstructural order, and particularly for the highest charge, one see very well defined stripes of C particles, stripes that now appear to be finite. A more clear picture emerges when taking a look at the partial structure factors, presented in left panels of Figure 10. Now, the prepeak is perfectly defined even for the S_{AA} structure factor for the lowest charge, in contrast with the uncharged system S_{AA}. The extremely large values of $S_{\alpha\beta}(k_0)$ for $k_0 \approx 0.25$ Å^{-1} resemble Bragg peaks and indicate the presence of quasi-periodic order in the microstructural domains. Moreover, if now one looks at the cluster size distributions plotted on the right panels of Figure 10, together with the percolating clusters, one finds now a maximum centered at $s \approx 20$ for $q = 0.25e$ for C and A-sites, which indicates the presence of finite clusters of monomers and A-sites. This maximum is preserved in the results obtained for other charges up to $q = 0.2e$ (not shown for the sake of brevity), to disappear for weaker Coulombic interactions. It is obvious that the net effect of charges on the microstructuring of our model mixture is to enhance the formation of nanostructures, also giving rise to the formation of finite size clusters for sufficiently high charges. In contrast, B-sites form a percolating bicontinuous structure coexisting with

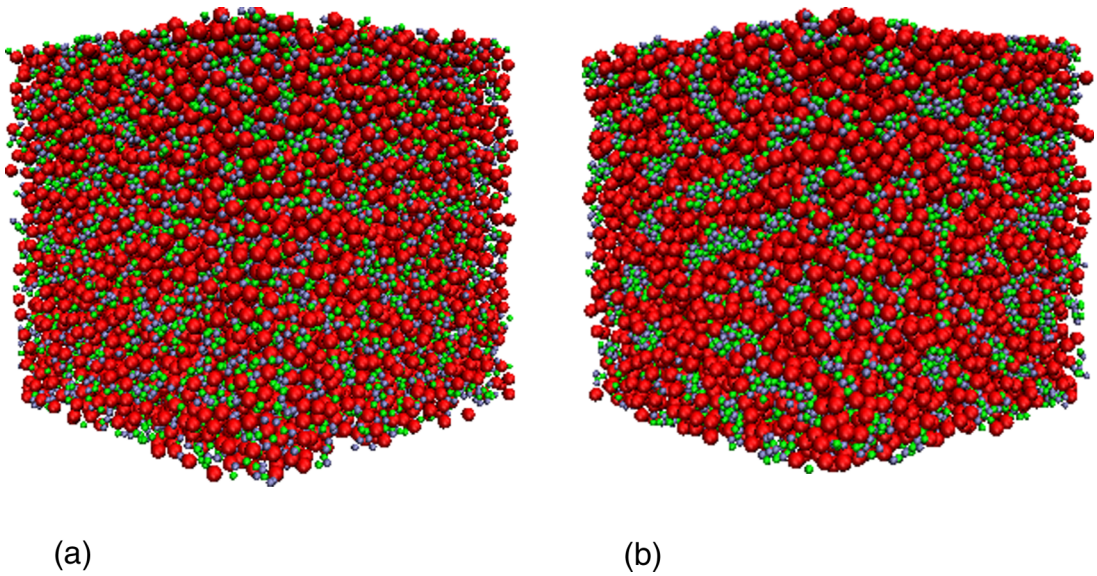

FIG. 9. Snapshots of the equimolar mixture of AB dimers and C monomers with embedded charges (indicated on the figures). (a) $q_A = 0.10e$; $q_C = -0.10e$. (b) $q_A = 0.25e$; $q_C = -0.25e$.

some disconnected B-sites or short lived aggregates. A-sites and C monomer form aggregates embedded in the percolating network of B-sites. All this suggests that the network of B-sites forms cavities, with the A-sites pointing inside the cavity. This in turn is filled by C monomers. This configuration is favored both by steric effects and by the net attraction between the positively charge A sites and negatively charged C monomers.

On the other hand, despite the fact that A-sites form part of the AB dimers and C monomers are independent particles, due to the symmetry of the electrostatic interactions and the symmetry in shape and density—$\sigma_{AA} = \sigma_{CC}$, $\rho_A = \rho_C$—as the charges increase, AA and CC correlations become extremely similar—compare S_{AA} and S_{CC} in Figure 10—as one would encounter in a simple fully symmetric electrolyte.

The next question is how this is all reflected on the effective potentials. These are plotted in Figure 11. In all cases, one observes the characteristic SALR structure, obviously being the CC and AA effective interactions those that are most affected by the introduction of charges. In spite of the fact that these two effective interactions result from the coarse graining of many body effects, the dominant role of electrostatic interactions already reflected in the partial structure factors leads to surprisingly similar effective potentials when charges are present. On the other hand, the changes in U_{BB}^{eff} are just quantitative.

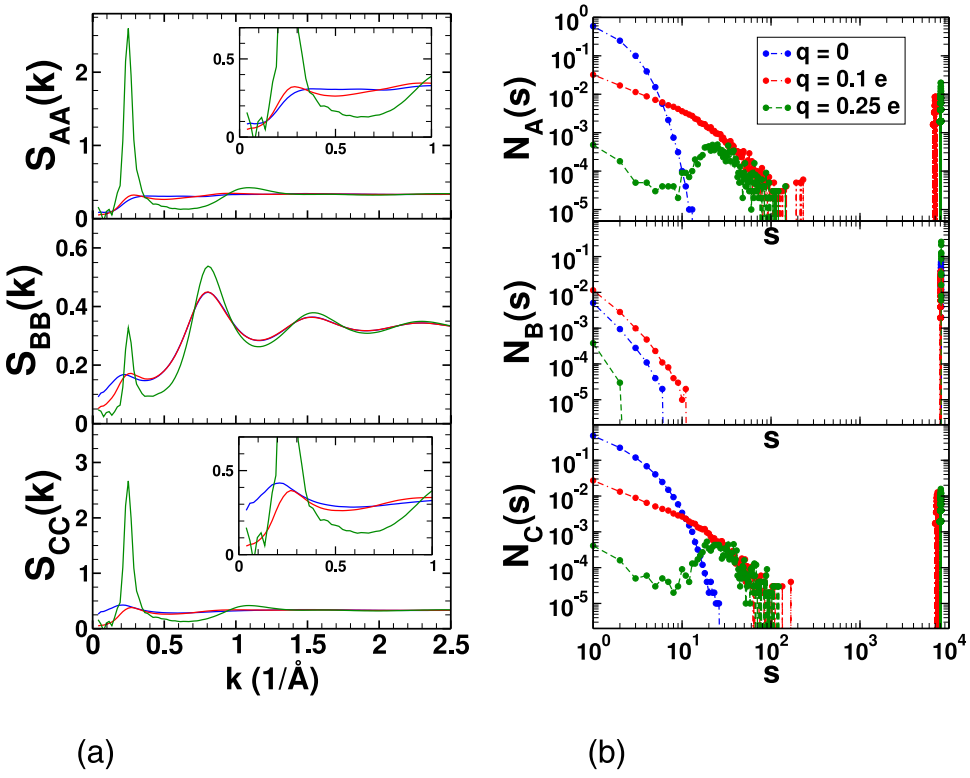

FIG. 10. (a) Charge dependence of the partial structure factors for A (top), B (middle), and C (bottom) particles. (b) Charge dependence of the cluster size distribution. Charge magnitudes are specified in the legend.

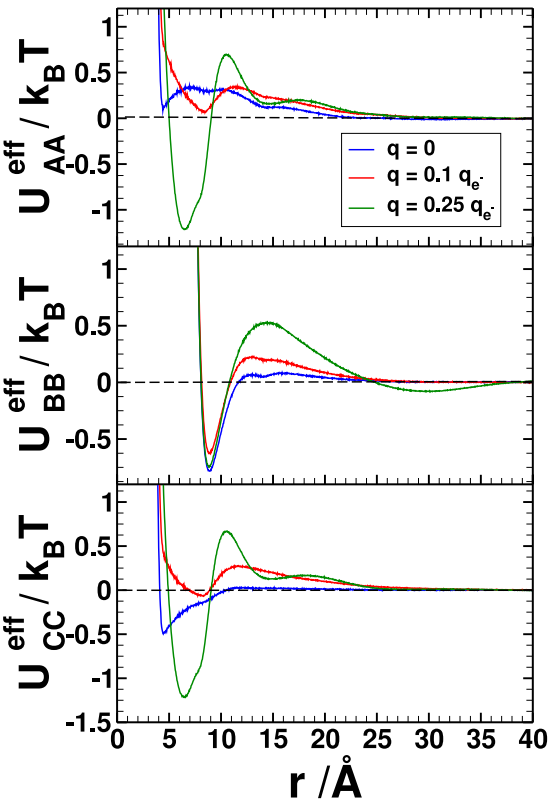

FIG. 11. Charge dependency of the effective potentials for A (top), B (middle) and C (bottom) particles. Charge magnitudes are specified in the legend. Values of r_{cl} correspond to the inflexion points of the effective potentials in their first minimum, i.e., $r_{cl}(A–A) = 6$ Å, $r_{cl}(B–B) = 11$ Å, and $r_{cl}(C–C) = 10$ Å.

The attractive part is hardly influenced by the charges, since it results mostly from the depletion interactions and the bare attractive u_{BB}. The long range repulsion is enhanced, and as the charge reaches $q = 0.25e$, oscillations appear. These oscillations recall the Friedel oscillations characteristic of effective cation-cation potentials in liquid metals.[46] In the latter instance, the oscillations result from the quantum nature of the electrons. Here, they result from the interplay of the Coulombic interactions and depletion forces. Thus, for sufficiently large charges, the long range attractive interaction between C and A sites propagates through the AB bonds and induces the attraction well around 30 Å as a result of a many body effect.

IV. CONCLUSIONS

In summary, we have shown that a simple mixture of heteronuclear AB dimers and C monomers, with short range attractive and repulsive interactions designed so as to mimic the interactions present in RTILs can give rise to the presence of nanostructural order in the form of micro-segregation in bicontinuous structures. This in turn translates into the characteristic presence of a prepeak in the site-site structure factors. These features are found both in simulation and in the integral equation results. The effective site-site potentials extracted from the pair distribution functions by means of an IMC and integral equation approach display the characteristic features of the SALR interactions, with the repulsive long range increasing as the total density (and hence the ordering) increases. The addition of charges to the model enhances the nanostructural order. When charges are large enough, one finds well structured phases in which bicontinuous structures coexist with finite size aggregates of monomers, caged in cavities formed by a network of the large uncharged sites and with the cationic sites facing the inner part of the cavity. The effect of charges on our simple and rather symmetric model induces the symmetrization of the correlations of the anionic monomers and the cationic sites. The microscopic structure formed by the uncharged sites (apolar head in the RTILs) retains its bicontinuous nature and even if it is stabilized and enhanced by the charges, it is still mostly dominated by depletion effects and the bare short range attraction of the B-sites. In this regard, it is interesting to note that the appearance of a prepeak in the wide angle scattering experiments and computer simulations of RTILS have been a subject of much investigations[47,48] and have been related to the charge ordering and the subsequent appearance of segregated charged and uncharged molecular domains. Our work presents a unified view of microsegregated bi-continuous domains, pre-peaks in structure factors, and SARL type interactions, which are common to many complex systems.

Obviously, a much richer variety of structures would result from longer attractive uncharged tails, beyond the single B-site model used here. On the other hand, our simple model when reduced to two dimensions most likely will also give rise to more complex structures, which in three dimensions are hindered by entropic effects. This is certainly a problem relevant to the behavior at interfaces which we intend to address in the future.

ACKNOWLEDGMENTS

C.B., N.G.A., and E.L. acknowledge financial support from the Dirección General de Investigación Científica y Técnica under Grant No. FIS2013-47350-C5-4-R. E.L. gratefully acknowledges the CNRS support of his stay at the LPTMC at the Université Pierre et Marie Curie, where most of this work was conceived.

[1]M. Seul and D. Andelman, Science **267**, 476 (1995).
[2]P. Godfrin, N. Valadez-Pérez, R. Castañeda-Priego, N. Wagner, and Y. Liu, Soft Matter **10**, 5061 (2014).
[3]N. G. Almarza, J. Pękalski, and A. Ciach, J. Chem. Phys. **140**, 164708 (2014).
[4]R. Mezzenga, P. Schurtenberger, A. Burbidge, and M. Michel, Nat. Mater. **4**, 729 (2005).
[5]M. Alexander, L. Rojas-Ochoa, M. Leser, and P. Schurtenberger, J. Colloid Interface Sci. **253**, 35 (2002).
[6]S. Yadav, T. Laue, D. Kalonia, S. Singh, and S. Shire, Mol. Pharmaceutics **9**, 791 (2012).
[7]E. Yearley, I. Zarraga, S. Shire, T. Scherer, Y. Gokam, N. Wagner, and L. Y., Biophys. J. **105**, 720 (2013).
[8]K. Johnston, J. Maynard, T. Truskett, A. Borwankar, M. Miller, B. Wilson, A. Dinin, T. Khan, and K. Kaczorowski, ACS Nano **6**, 1357 (2012).
[9]S. Choi, K. Wang, M. Leung, G. Stupian, N. Presser, S. Chung, G. Markovich, S. Kim, and J. Heath, J. Vac. Sci. Technol. **17**, 1425 (1999).
[10]P. Charbonneau and D. Reichman, Phys. Rev. E **75**, 050401 (2007).
[11]C. P. Royall, W. C. K. Poone, and E. R. Weeks, Soft Matter **9**, 17 (2013).
[12]P. Segre, V. Prasad, A. Schofield, and D. Weitz, Phys. Rev. Lett. **86**, 6042 (2001).

[13]W. Poon, A. Pirie, M. Haw, and P. Pusey, Physica A **235**, 110 (1997).
[14]A. Stradner, H. Sedgwick, F. Cardinaux, W. Poon, S. Edelhaaf, and P. Schurtenberger, Nature **432**, 492 (2004).
[15]J. Groenewold and W. K. Kegel, J. Phys. Chem. B **105**, 11702 (2001).
[16]J. Canongia Lopes and A. Pádua, J. Phys. Chem. B **110**, 3330 (2006).
[17]P. J. Camp, Phys. Rev. E **68**, 061506 (2003).
[18]B. Derjaguin and L. Landau, Appl. Sci. Res., Sect. B **14**, 633 (1941).
[19]E. Verwey and J. Overbeek, *Theory of the Stability of Lyophobic Colloids* (Elsevier, Amsterdam, 1948).
[20]J. Bomont, J. Bretonnet, D. Costa, and J. Hansen, J. Chem. Phys. **137**, 011101 (2012).
[21]P. Godfrin, R. Castañeda-Priego, Y. Liu, and N. Wagner, J. Chem. Phys. **139**, 154904 (2013).
[22]F. Sciortino, S. Mossa, E. Zaccarelli, and P. Tartaglia, Phys. Rev. Lett. **93**, 055701 (2004).
[23]E. Mani, W. Lechner, W. Kegel, and P. Bolhuis, Soft Matter **10**, 4479 (2014).
[24]R. Sear, S. Chung, G. Markovick, W. Gelbart, and J. Heath, Phys. Rev. E **59**, R6255 (1999).
[25]A. Imperio and L. Reatto, J. Phys.: Condens. Matter **16**, S3769 (2004).
[26]A. Imperio and L. Reatto, J. Chem. Phys. **124**, 164712 (2006).
[27]D. Schwanzer and G. Kahl, J. Phys.: Condens. Matter **22**, 415103 (2012).
[28]A. Archer, Phys. Rev. E **78**, 031402 (2008).
[29]E. Lomba, C. Bores, and G. Kahl, J. Chem. Phys. **141**, 164704 (2014).
[30]A. Meyra, G. Zarragoicoechea, and V. Kuz, Mol. Phys. **110**, 173 (2012).
[31]N. G. Almarza and E. Lomba, Phys. Rev. E **68**, 011202 (2003).
[32]C. Merlet, M. Salanne, and B. Rotenberg, J. Phys. Chem. C **116**, 7687 (2012).
[33]J. Weeks, D. Chandler, and H. Andersen, J. Chem. Phys. **54**, 5237 (1971).
[34]S. Plimpton and A. Thompson, MRS Bull. **37**, 513 (2012).
[35]S. Plimpton, J. Comput. Phys. **117**, 1 (1995).
[36]M. Brown, P. Wang, S. Plimpton, and A. Tharrington, Comput. Phys. Commun. **182**, 898 (2011).
[37]D. Frenkel and B. Smit, *Understanding Molecular Simulation* (Academic, London, 2002).
[38]A. Bathia and D. Thornton, Phys. Rev. E **2**, 3004 (1970).
[39]J.-P. Hansen and I. McDonald, *Theory of Simple Liquids*, 2nd ed. (Academic, London, 1990).
[40]B. Kezic and A. Perera, J. Chem. Phys. **135**, 234104 (2011).
[41]J.-P. Hansen and L. Verlet, Phys. Rev. **184**, 151 (1969).
[42]A. Perera and B. Kežić, Faraday Discuss. **167**, 145 (2013).
[43]A. Perera and R. Mazighi, "Simple and complex forms of disorder in ionic liquids," J. Mol. Liq. (published online).
[44]S. Izvekov, M. Parrinello, C. J. Burnham, and G. A. Voth, J. Chem. Phys. **120**, 10806 (2004).
[45]D. Stauffer, Phys. Rep. **54**, 1 (1979).
[46]N. Cusack, *The Physics of Structurally Disordered Matter: An Introduction*, 2nd ed. (Adam Hilger, Bristol, 1987).
[47]H. V. R. Annapureddy, H. K. Kashyap, P. M. D. Biase, and C. J. Margulis, J. Phys. Chem. B **114**, 16838–16846 (2010).
[48]Y. Wang, W. Jiang, T. Yan, and G. A. Voth, Acc. Chem. Res. **40**, 1193–1199 (2007).